Finite element modeling of a superconducting fault current limiter

Lale ERGENE[1,*]**, J. Keith NELSON**[2]**, Raghunath PARTHASARATHI**[2]
[1]*Department of Electrical Engineering, Faculty of Electrical and Electronic Engineering,*
İstanbul Technical University, 34469 İstanbul-TURKEY
e-mails: ergenel@itu.edu.tr
[2]*Rensselaer Polytechnic Institute, Electrical Power Engineering,*
Troy, New York 12180-USA
e-mails: nelson@rpi.edu, parthr@rpi.edu

Abstract

This paper summarizes the work done to show finite element modeling results on a high temperature superconductor fault current limiter (FCL). The paper also gives the small mock-up design of the matrix FCL and its finite element model (FEM). It also discusses the limitations of the FEM and explains how the results from the FEM compare with the experimental data derived for the configuration. A 3-dimensional FEM has been used because of the structure of the real geometry, which does not show any plane or axisymmetric features.

Key Words: *Finite element method, high temperature superconductor, resistive limited fault current limiter, transient analysis*

1. Introduction

Even though high-temperature superconductor (HTS)-type limiters were developed in late 1980s, there are not many practical and low-cost solutions in the applications [1,2]. HTS materials show zero resistance below a critical temperature, T_c. A fault current limiter (FCL) limits the fault current at the desired level. One application of the HTS materials is the FCL to control the fault current in power networks. An HTS FCL shows a no-loss feature under normal operating conditions. However, it will be quenched from the superconducting state to the conducting state when a fault occurs. There will be zero resistance at the superconducting state and high resistance after the quench to limit the fault current. There are numerous approaches that may be employed in order to utilize the unique properties of superconductivity in fabricating a FCL for power system networks, where fault levels may exceed circuit breaker capability. Some of the options available have been reviewed by Salasoo et al. [3], Leung [4], and Kovalsky et al. [5]. Depending on the design, superconducting FCLs

---

*Corresponding author: Department of Electrical Engineering, Faculty of Electrical and Electronic Engineering, İstanbul Technical University, 34469 İstanbul-TURKEY

often have extra desirable characteristics in addition to the basic function of adding circuit impedance under fault conditions. Such attributes may include fast transition from the normal to limiting state, fast recovery to normal operation after a fault is interrupted, insensitivity to normal overload currents, discharging of capacitor banks, high dielectric strength to transient overvoltages during a current limiting operation, compact size, light weight, low cost, and highly reliability with minimum maintenance [6]. Resistive FCL designs, which rely on the quenching of HTS elements in order to insert impedance into the network, are clearly attractive since they can utilize the quench phenomenon described by Eqs. (1) and (2) in the Appendix to automatically detect an overcurrent and insert impedance. However, a series connection of HTS rods used for this purpose needs to ensure that the elements switch rapidly and simultaneously for reliable operation. One method to do that is to capitalize on the fact that J_c in Eq. (1) is dependent on the local magnetic field. By using trigger coils around the HTS elements in the manner shown in Figure 1, this can be achieved and will minimize the occurrence of destructive hot spots.
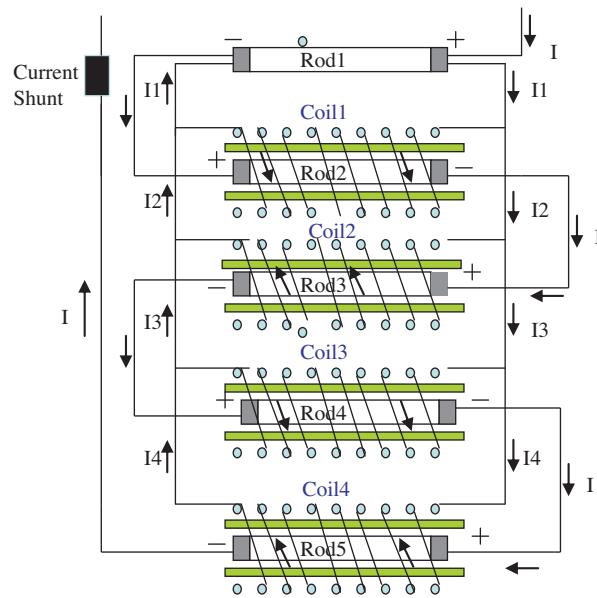

Figure 1. The laboratory configuration.

However, the design of such a system is not straightforward since the trigger currents, and the resulting magnetic fields, depend on the induction and thus on the specific layout of the components. As a result, a detailed model is needed in order to effectively design a practical device. This study seeks to create a finite element model (FEM) for this purpose and verify its predictions by comparison with experimental results from a small laboratory representation of an HTS FCL, which is designed for a 138-kV high-voltage transmission line. The first phase of the study is to create a FEM for the new design of a FCL, both to understand how the test mock-up design works and to provide insight to refine the design. The proposed FEM models are focused on the resistive type of superconducting FCL [6-8]. The superconducting material behavior due to the external magnetic field is taken into account. Assumptions are made to model the superconductor material features because of software limitations. These limitations are the inability to couple solid conductors to the external circuit, inability to depart from cryogenic temperature, etc.

Thus, the regular coil is used instead of solid coil for the HTS elements. These FEMs are magnetic models and do not account for any departures from the nominal cryogenic temperature (77 K).

Therefore, resistances represent the superconducting elements in the external circuit. In order to model insertion of a superconducting device (such as a coil) in an electric circuit, coupling with the circuit equations is also required. The model simultaneously solves the finite element equations of A-Ψ formulation and the circuit equations [9]. The real laboratory test setup is represented in the FEM, which includes a capacitor as an initial voltage source, the switching process to initiate the simulated fault current, and the resistance and inductance of the system. These external components are coupled to the 3-D FEM to allow a dynamic representation of FCL operation. An automatic mesh generator is used and controlled manually by inserting more elements where the places need denser element distribution. The mesh should be fine in the regions where the flux density and/or current density change rapidly. This study was done using the time-dependent (transient) formulation with the external circuit connection.

2.   Description of the laboratory design

The mock-up design is created to test material properties and compare experimental results with the FEM findings. Figure 1 shows 5 series-connected HTS elements [based on $Bi_2Sr_2CaCu_2O_{8+\delta}$ (a.k.a. BSCCO or Bi-2212) rods] with parallel-connected trigger coils. The HTS rods are 100 mm in length and 10 mm in diameter. In this configuration, the first HTS rod (labeled Rod1 in Figure 1) is the trigger element and the other 4 HTS elements behave as limiting elements. The trigger coils are wound around the HTS elements and they are connected in parallel across the trigger element.
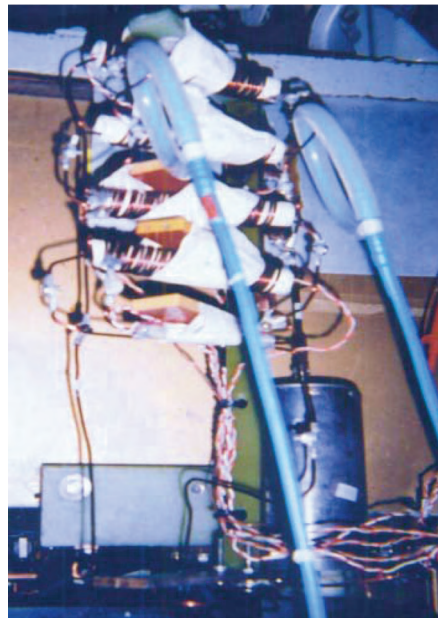

Figure 2. The experimental setup.

In Figure 1, I is the main current, and I1, I2, I3, and I4 are the currents in trigger loops 1, 2, 3, and 4, respectively. There are 4 magnetic coils around the HTS cylinders. In this model, the magnetic coils are represented as a bulk coil. Each of them has 7 turns, as the real model does. The arrow directions indicated are the initial assumed positive directions. Since this experiment is based on a 5-kA, 390-Hz oscillatory pulse current, the FEM model also simulates a 390-Hz pulsating main current frequency. The test configuration is shown in Figure 2.

All of the circuit elements are immersed in LN_2 and the currents in the circuit are measured using Rogowski coils.

3. Finite element model

The FEM is a powerful and widely used numerical method for the solutions of partial differential equations. This method can be used to solve partial differential equations of real engineering problems in different disciplines such as mechanical, electrical, civil, etc. The method essentially consists of a continuous function for the solution. In this method, the given continuous problem is first discretized, then a system of equations with finite dimensions is generated, and finally the approximate solution is obtained by solving the resulting linear system of the equations [9]. The method has also been used to model different types of superconducting FCLs in recent years [10,11]. In this paper, the FEM is used to model a test design and the results are compared with the experimental data derived for the configuration.

Figures 3a and 3b show the FEM geometry of the mock-up configuration corresponding to Figure 1. Since 2-D modeling of the software supports either plain or axisymmetric problems, 3-D finite element modeling is unavoidable for this type of the geometry. Three-dimensional modeling also helps to determine the flux density components (B_x, B_y, B_z) for each magnetic coil. Each cylinder in Figure 3b represents an HTS element series connected to the external electric circuit. The arrows inside the coils in Figure 3a refer the direction of the current for each HTS element. There are magnetic coils around the lower 4 HTS cylinders. These are connected to the external circuit as well. In Figure 3, there is an outer box around the test configuration. This represents the infinite boundary where the flux values extend to 0. In this model, each magnetic coil has 7 turns, as in the experimental model. The automatic mesh generator is augmented manually by inserting mesh density in the places needing a denser element distribution, such as the areas surrounding the HTS elements. The mesh consists of 40,000 second-order volume elements connected to 54,000 nodes.
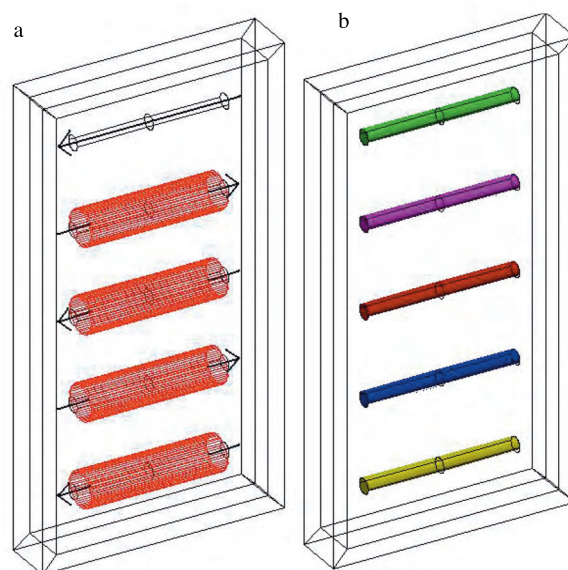

Figure 3. The FEM configuration: a) magnetic coils and b) HTS elements.

Figure 4 shows the external circuit diagram created in the finite element program. In this circuit, a capacitor is used as a voltage source. It is initially charged to 2.3 kV and there is a switch included to control capacitor discharge. The main circuit impedance is represented by inductance and resistance, which are in series to the electrical switch as shown in Figure 4. Each HTS element and magnetic coil is represented by its circuit inductance and resistance in series with its coil representation. The coil permits connection of the electrical circuit to the magnetic circuit in the software. The external circuit allows the one to couple the electric circuit to the magnetic problem in finite elements. Magnetic and electrical equations are solved simultaneously in the time domain using this coupling feature. Thus, magnetic field results such as flux density values at any point, flux density distribution in any region, magnetic field values, magnetic field vectors, and equiflux lines can be postprocessed at any time during the computing, while the electrical circuit quantities such as coil currents and voltages can be postprocessed at the same time. To compute the loop currents accurately, the parasitic elements between the magnetic coils are also included in the electrical circuit. Coupling between coils is accounted for by mutual terms automatically by the FEM software [12,13]. This aspect is important since it was assumed that the anomalous current behavior in the trigger coil resulted from the interaction of the intended driving current from the first trigger element after the quench with the induced currents flowing in the main circuit. The closely coupled nature of the trigger coils to the HTS elements makes this the principal source of induction. Some voltage will also be induced in the end region, but the flux diverges rapidly there. Since the representation of coils in the model will provide an average of the B-field, the induced components of voltage can be calculated externally. These induced voltages are computed and injected into the external circuit as a voltage source for each loop. These applied voltages are iterated in the FEM to get a sufficient convergence. The current in the main circuit (I) produces a varying magnetic field along the length of the coil. The winding angle (θ) of the trigger coils causes the dot product in Faraday's law to generate a cumulative coil voltage when interacting with the main circuit azimuthal flux.
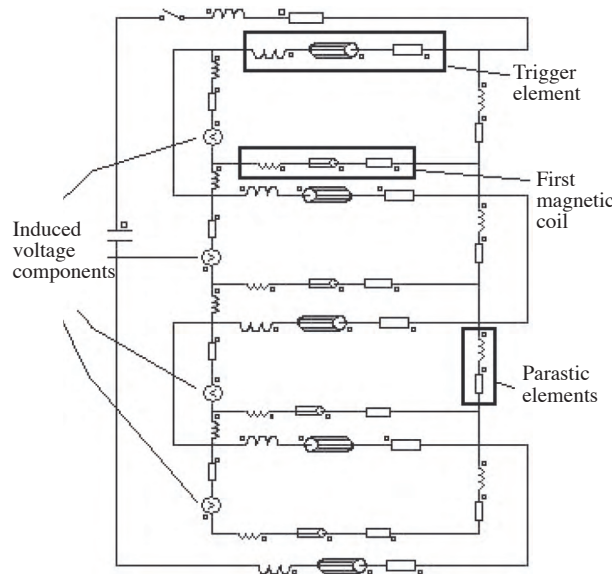

Figure 4. Electrical circuit connected to the FEM.

In the external circuit, the induced effect cannot be observed since the magnetic coil is defined as a bulk coil. This is another limitation of the modeling.

4.   Results

Figure 5 shows the initial capacitor discharging voltage and currents during the quench of the HTS elements in a fault limiting situation. The natural frequency of the experimental system is 390 Hz and the FEM also gives the solution at approximately that frequency. The initial voltage of the capacitor is 2.3 kV.
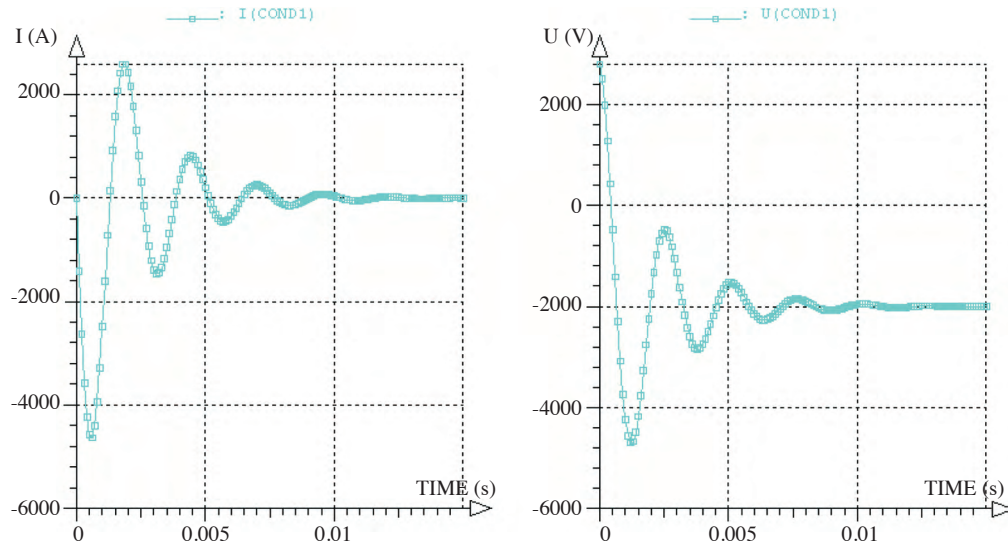

Figure 5. Capacitor current and voltage transients.

Figure 6 shows magnetic field vectors for 2 different phases of solution. Since the magnetic coils and HTS elements are carrying currents in different directions (HTS elements conduct in the z-direction, while magnetic coils conduct in the azimuthal direction), the combined magnetic field effect can be seen in 2 directions. Since the first HTS element (trigger element) is parallel with the magnetic coils, this element carries less current
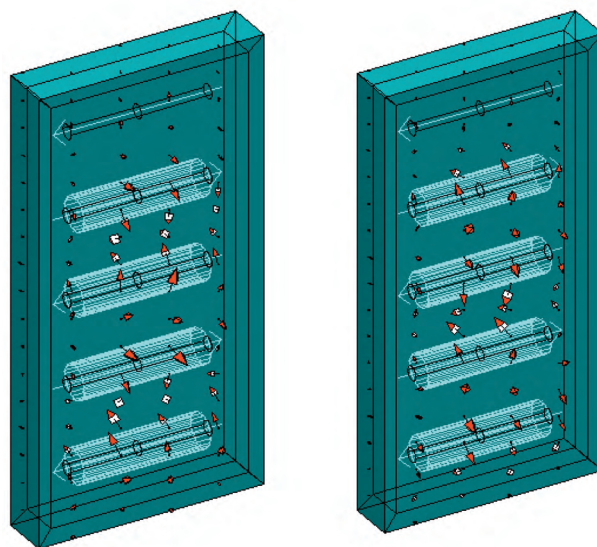

Figure 6. Magnetic field vectors at different instants of time: a) t = 3 ms and b) t = 8 ms.

compared to the other HTS elements. Less current creates fewer magnetic fields around the first HTS element, and this can be observed in Figure 6. The top portion of the problem domain has smaller vectors compared to the rest of the model. The other HTS elements are in series. They are carrying the same amount of the current, which will create the same amount of flux around the HTS elements.

Figure 7 shows the flux density distribution for the problem domain when the main circuit current is peaking (5 kA).
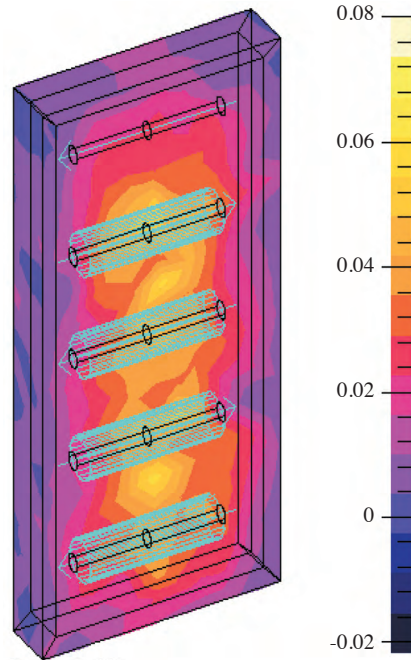

Figure 7. Flux density distribution in tesla (T) at the main circuit peak current.
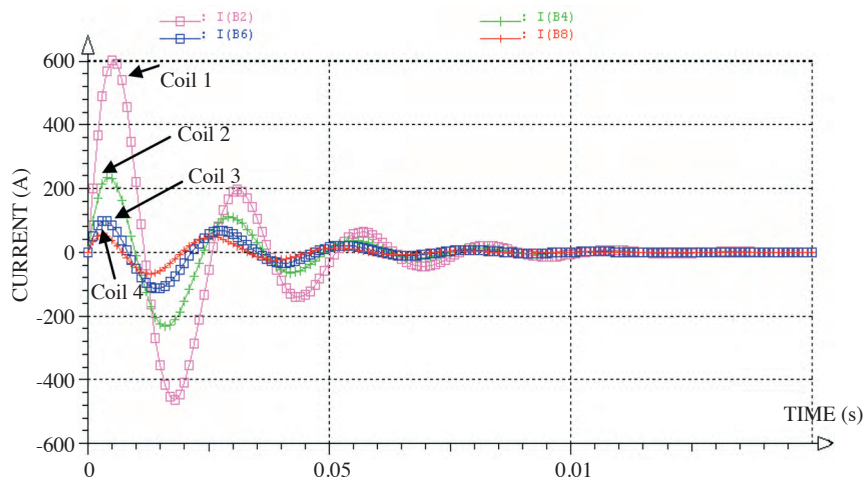

Figure 8. Computed magnetic coil currents.

Figure 7 also shows that the magnetic field is similar for all of the elements except the trigger element. As the legend shows, the lighter shades refer to the higher flux density. The values are given in tesla (T). The conduction current components of the magnetic coils are shown in Figure 8. B2 refers to the 1st magnetic coil,

B4 is the 2nd, and B6 and B8 are the 3rd and 4th. Figure 9 shows the main current and the 1st coil current after the quench.
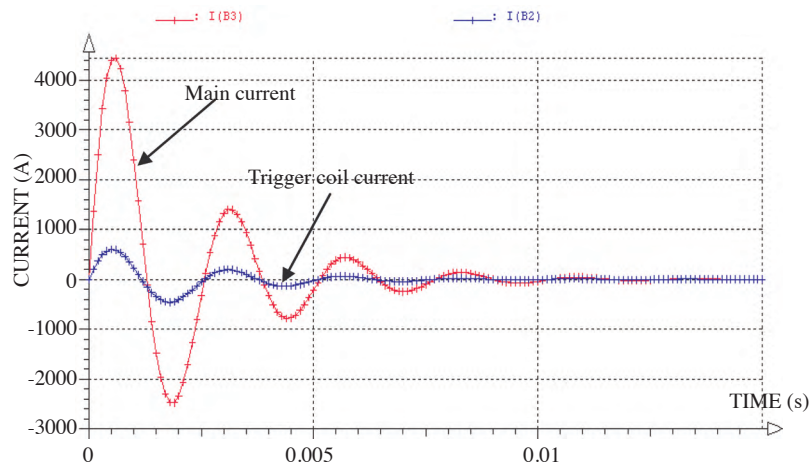

Figure 9. Relationship between the main current and 1st coil current after the quench. B2: 1st magnetic coil, B3: 2nd HTS element (carries main circuit current).

The test and FEM analysis for the main circuit currents are shown in Figure 10. The first peak of the current at the beginning of the quench is well represented, although the decay decrement is a little different. However, in light of the complexity of the 3-D interactions involved, the model would appear to be useful.

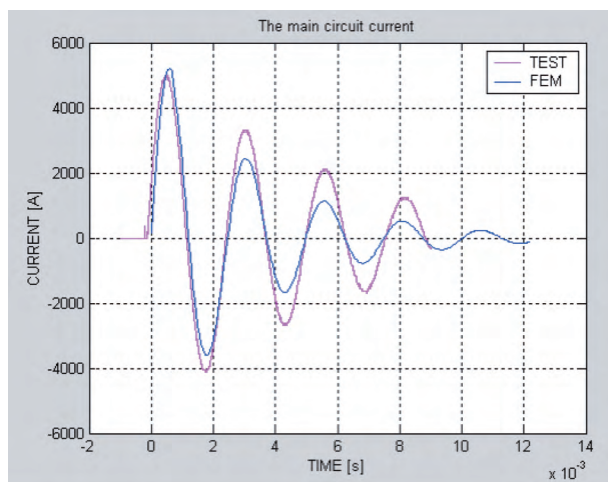Figure 11 shows the voltage drop across the first HTS element for the test and FEM results.

Figure 10. Main circuit current for the test and FEM.
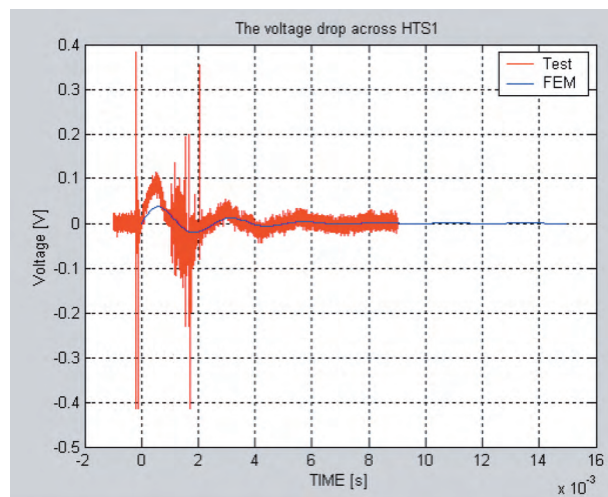

Figure 11. Voltage drop across the first HTS element.

On the given path in Figure 12, the magnetic field has 3 components. The azimuthal B-field, due to the main current, has the biggest effect. It alternates in direction since the components are connected in a serpentine fashion. The axial B-field is due to trigger current. The x-axis refers to the length of the path (in meters) and the y-axis is the flux density for the 3 components (in tesla).
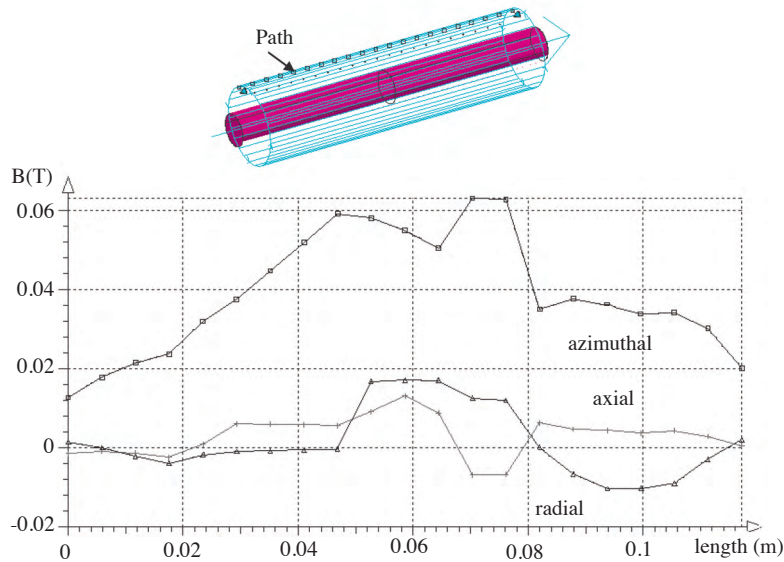
Figure 12. The flux density components on the first magnetic coil for the given path.

After including the induced currents into the model, the coil current is dramatically changed. Figure 13 shows the magnetic coil currents corresponding to a 5-kA main circuit current for the entire model.
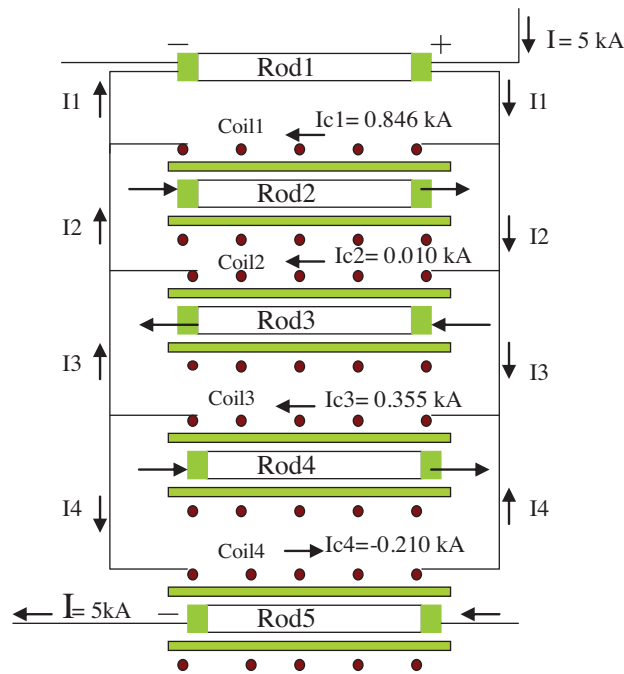

Figure 13. The coil currents after including the induced components.

The conduction and induced and resultant current components for each coil are given in the Table for the test and the FEM. The comparison verifies the current directions. The fourth magnetic coil current is assigned a negative sign because the current is flowing in the opposite direction of the initially assumed positive direction. The induced currents are almost equal and the value of the conduction component of the current in the magnetic coil circuits decreases rapidly with the distance of the coil from the trigger element.

850

Table. Peak coil currents (in kA).

Main I (= 5 kA)	Model conduction	Model induced	Model total	Test
Coil 1	0.59	0.26	0.85	0.84
Coil 2	0.2	−0.2	0.01	0.02
Coil 3	0.064	0.3	0.36	0.46
Coil 4	0.020	−0.23	−0.21	−0.3

Figure 14 shows the flux density distribution with the induced current components included when the main circuit current is at its peak. This is different from that of Figure 7 and the last coil is devoid of flux due to the interactions.
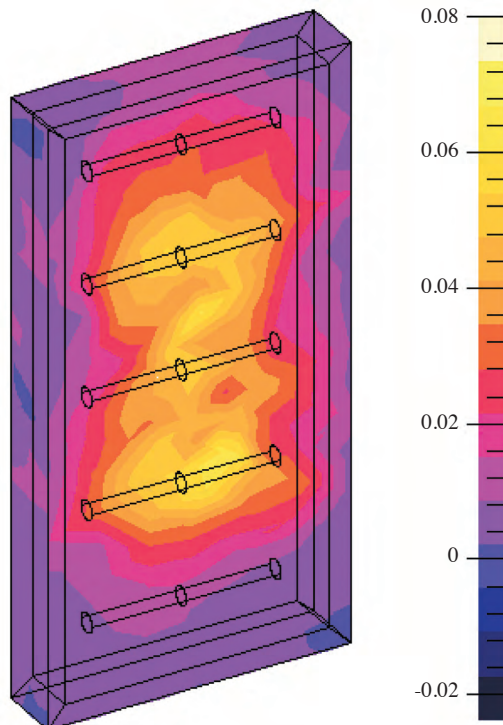

Figure 14. Flux density distribution in tesla (T) at 5 kA main peak circuit current with the induced components.

5.   Conclusion

In a FCL configuration in which the HTS elements have surrounding coils to provide feedback for the superconducting quench process, the coil currents are substantially altered by the induced voltages. Although the predicted currents only approximately line up with the experimental values, the order of magnitude is correct and the polarities and characteristics are all replicated. The induced and conduction components of the B-field have been established together with their 3-D distribution over the HTS elements. This aspect is important in the design of a FCL, which relies on the homogeneous quench of series elements. As a "sanity check", computed flux densities were checked against approximate hand-calculated values. Although the HTS material quench was modeled nondynamically since the thermal effects were not included, induced voltages were computed on the basis of the flux distribution by iteratively including them in the external circuit to circulate currents to

cancel those from the trigger elements.

Clearly, having developed (and experimentally verified) the methodology on a device of limited size, there is now confidence in applying the method in the design of a full-size FCL configured with similar serpentine HTS elements. The full-size design model will obviously embody a greater number of elements and have somewhat different dimensions, but will be based on the FEM tools developed here, which provide the flexibility to allow for changes in material properties, coil structures, etc. In the application to the actual device, the system would be represented by its Thevenin equivalent instead of the charged test capacitor and shaping inductor used in the laboratory verification apparatus.

Appendix

HTS material modeling with FEM

The constitutive laws of HTS material are expressed as follows:

$$\vec{B} = \mu_0 \vec{H}, \tag{1}$$

$$\vec{E} = \rho(J, B)\vec{J}. \tag{2}$$

One of the formulae representing the electrical behavior of the HTS material is a law expressed with a power dependence that is near the critical current density, J_c. This law is the nonlinear electromagnetic E-J power law, which was initially proposed by Rhyner [14].

$$\vec{E} = E_c \left(\frac{J}{J_c}\right)^{N-1} \frac{\vec{J}}{J_c} \tag{3}$$

Here, E_c is the critical electric field and N is a parameter chosen so that this law approaches the experimental characteristic as accurately as possible. The resistivity dependence of the material may be expressed as given below.

$$\rho_1 = \frac{E_c^{1/N}}{J_c} |E|^{(1-1/N)} \tag{4}$$

ρ_0 is the finite residual resistivity, which is defined for numerical stability. The total resistivity is given below.

$$\rho = \rho_0 + \rho_1 \tag{5}$$

The HTS properties are described by the following constants:

$\rho_0 : 1 \times 10^{13}$ S/m

J_c: 4.4×10^7 A/m^2

E_c: 1×10^{-4} V/m

N: 15

Nomenclature

FCL	Fault current limiter
HTS	High temperature superconductor
LN$_2$	Liquid nitrogen
T_C	Critical temperature
A	Magnetic vector potential
Ψ	Time-integrated electric scalar potential
B	Magnetic flux density
H	Magnetic field

H_C	Critical magnetic field	N	Power index from the fit
E_C	Critical current	ρ_1	Nonlinear resistivity
J_C	Critical current density	ρ_0	Finite residual resistivity
$|\mathbf{E}|$	Module of the electric field	ρ	Total nonlinear resistivity
J	Current density		

References

[1] E. Thuries, V.D. Pham, Y. Laumond, T. Verhaege, A. Fevrier, M. Collet, M. Bekhaled, "Towards the superconducting fault current limiter", IEEE Transactions on Power Delivery, Vol. 6, pp. 801-808, 1991.

[2] D. Ito, E.S. Yoneda, K. Tsurunaga, T. Tada, T. Hara, T. Ohkuma, T. Yamamoto, "6.6 kV/1.5 kA-class superconducting fault current limiter development", IEEE Transactions on Magnetics, Vol. 28, pp. 438-44, 1992.

[3] L. Salasoo, A.F. Imece, R.W. Delmerico, R.D. Wyatt, "Comparison of superconducting fault limiter concepts in electric utility applications", IEEE Transactions on Applied Superconductivity, Vol. 5, pp. 1079-1082, 1995.

[4] E. Leung, "Superconducting fault current limiters", IEEE Power Engineering Review, Vol. 20, pp. 15-18, 2000.

[5] L. Kovalsky, X. Yuan, K. Tekletsadik, A. Keri, J. Bock, F. Breuer, "Applications of superconducting fault current limiters in electric power transmission systems", IEEE Transactions on Applied Superconductivity, Vol. 15, pp. 2130-2133, 2005.

[6] K. Tekletsadik, M.P. Saravolac, A. Rowley, "Development of a 7.5 MVA superconducting fault current limiter", IEEE Transactions on Applied Superconductivity, Vol. 9, pp. 672-675, 1999.

[7] S. Elschner, F. Breuer, A. Wolf, M. Noe, L. Cowey, J. Bock, "Characterization of BSCCO 2212 bulk material for resistive current limiters", IEEE Transactions on Applied Superconductivity, Vol. 11, pp. 2507-2510, 2001.

[8] B. Gromoll, G. Ries, W. Schmidt, H.P. Kraemer, B. Seebacher, B. Utz, R. Nies, H.W. Neumueller, E. Baltzer, S. Fischer, B. Heismann, "Resistive fault current limiters with YBCO films - 100 kVA functional model", IEEE Transactions on Applied Superconductivity, Vol. 12, pp. 656-659, 2002.

[9] S. Salon, M.V.K. Chari, Numerical Methods in Electromagnetism, San Diego, Academic Press, 1999.

[10] Y.J. Kim, D.K. Park, S.E. Yang, W.C. Kim, M.C. Ahn, Y.S. Yoon, N.Y. Kwon, H. Lee, T.K. Ko, "Analytical design method of high-T_c coated conductor for a resistive superconducting fault current limiter using finite element method", IEEE Transactions on Applied Superconductivity, Vol. 20, pp. 1172-1176, 2010.

[11] F. Moriconi, N. Koshnick, F. De La Rosa, A. Singh, "Modeling and test validation of a 15 kV, 24 MVA superconducting fault current limiter", IEEE Transmission and Distribution Conference and Exposition, pp. 1-6, 2010.

[12] E. Vinot, V. Leconte, G. Meunier, P. Tixador, "Circuit coupling method applied to bulk superconductors," IEEE Transactions on Magnetics, Vol. 38, pp. 3661-3664, 2002.

[13] G. Rubinacci, A. Tamburrino, F. Villone, "Three dimensional finite elements modeling of superconductors", IEEE Transactions on Magnetics, Vol. 36, pp. 1276-1279, 2000.

[14] J. Rhyner, "Magnetic properties and AC-losses of superconductors with power law current-voltage characteristics", Physica C: Superconductivity, Vol. 212, pp. 292-300, 1993.